

## Effect of Ga<sub>2</sub>O<sub>2</sub>-graphene heterostructures on methyl blue degradation in wastewater

Bassam Al-Faqiri<sup>a</sup>, M. Rashad<sup>a,b,\*</sup>, Sultan Al-Osaimi<sup>a</sup>, Abdullah Al-Ghamdi<sup>a</sup>, Fahad A. Al-Shehri<sup>a</sup>, Mohammed M. Al-Belwi<sup>a</sup>, S.A. Al-Ghamdi<sup>a</sup>, Nagih M. Shaalan<sup>b,c</sup>

<sup>a</sup>Physics Department, Faculty of Science, University of Tabuk, Tabuk 71491, Saudi Arabia, emails: m.ahmad@ut.edu.sa (M. Rashad), bsaaam37@gmail.com (B. Al-Faqiri), sa5690178@gmail.com (S. Al-Osaimi), aalghamdi@ut.edu.sa (A. Al-Ghamdi), fahad.almosbeh@gmail.com (F.A. Al-Shehri), moh.albelwi92@gmail.com (M.M. Al-Belwi), saalghamdi@ut.edu.sa (S.A. Al-Ghamdi)

<sup>b</sup>Physics Department, Faculty of Science, Assiut University, Assiut 71516, Egypt, email: nmohammed@kfu.edu.sa (N.M. Shaalan)

<sup>c</sup>Department of Physics, College of Science, King Faisal University, P.O. Box: 400, Al-Ahsa 31982, Saudi Arabia

Received 30 December 2022; Accepted 12 May 2023

### ABSTRACT

Gallium oxide (Ga<sub>2</sub>O<sub>2</sub>) nanoparticles (NPs) were fabricated using chemical method. We looked at how two distinct graphene concentrations in a gallium oxide-graphene (Ga<sub>2</sub>O<sub>2</sub>/graphene) heterostructure nanocomposite affected the photocatalytic degradation of the methyl blue dye. Raman spectroscopy was used to evaluate some of the prepared Ga<sub>2</sub>O<sub>2</sub> NPs' physical characteristics. On the basis of interactions between Ga<sub>2</sub>O<sub>2</sub> and graphene, the effect was examined. Ga<sub>2</sub>O<sub>2</sub> included the laser-induced graphene. The production of disordered graphene and the phase of oxides and graphene were both validated by Raman spectra. Ga<sub>2</sub>O<sub>2</sub> was used to examine the effects of graphene content at 5 and 10% wt. The results of the photocatalysis measurements showed an improvement, but a 10% addition of graphene led to a remarkable improvement. The results indicated that the photocatalytic application of the binary phase of Ga<sub>2</sub>O<sub>2</sub>/graphene toward the methyl blue decomposition is promising.

**Keywords:** Ga<sub>2</sub>O<sub>2</sub> heterojunction; Binary nanocomposite; Graphene; Methyl blue; Photocatalytic; Adsorption

### 1. Introduction

All areas of research have been affected by nanotechnology, with occasional successes being noted. When a material is reduced to nanoscale, it acquires an excessive number of additional specifications, including those related to edge density, internal structure, lattice symmetry, and cell characteristics [1]. In recent years, metal oxide nanoparticles have gained popularity due to their distinctive characteristics, such as their huge surface area, enhanced activity, and electrical properties [2,3]. Semiconducting oxides based on the photocatalytic process have drawn a lot of interest as an environmentally beneficial, economically

feasible, and long-lasting water purification method [4]. It has long been known that improved oxidation technology can eliminate microorganisms and persistent organic pollutants from water [5]. The process takes place on the surface of a photocatalytic layer, in accordance with the streamlined Langmuir–Hinshelwood kinetic model [6]. Therefore, any increase in active surface area or modification of the geometry of the oxide's structure will improve the performance of the oxide. Finding methods to remove methylene blue (MB) from wastewater is crucial since it is a chemical with a complex aromatic makeup that is resistant to degradation. Due to their significant features, including as high surface area, carbon-based materials, like graphene

\* Corresponding author.

and low graphene oxide (RG), are essential in a variety of fields, including lithium-ion batteries, nanosensors, and energy storage applications [7–10]. In instance, the indirect semiconductor  $\text{Ga}_2\text{O}_3$  monolayer has a broad band gap of 2.752 eV and a high hole mobility of  $4,720 \text{ cm}^2/\text{V}\cdot\text{s}$ . By using applied strain and layer control, its band gap may be controlled flexibly across a wide range. In the UV region, it has strong absorption coefficients ( $>10^5 \text{ cm}^{-1}$ ) [11]. Because to the formation of potent reactive radicals including hydroxyl radicals ( $\cdot\text{OH}$ ) and superoxide radicals  $\cdot\text{O}_2^-$ , it is a good material for photocatalytic reactions. Due to its high  $E_g$  value, it can only function in the presence of UV light, making insufficient use of visible light [12]. Due to the increased number of active sites, several different dimensional configurations, including nanoparticles (0-D), nanowires/nanorods/nanotubes (1-D), nanoflakes/nanosheets (2-D), and nanospheres/nanoflowers (3-D), have been identified as promising photocatalysts [13]. To investigate the impact of heterojunction of graphene and  $\text{Ga}_2\text{O}_3$  content on the performance toward two MB concentrations of 5 and 10 mg/L.  $\text{Ga}_2\text{O}_3/5\%\text{Gr}$  and  $\text{Ga}_2\text{O}_3/10\%\text{Gr}$  heterostructure nanocomposites are created in this work. The Raman spectroscopy is used to analyze the structural composition. The Raman spectroscopy is used to analyze the structural composition. To clarify the impact of the binary composition, the efficiency was calculated for a variety of compositions.

## 2. Experimental technique

### 2.1. Materials preparation

In the current preparation procedure, 25 mL of a 0.2 M copper nitrate solution ( $\text{Ga}(\text{NO}_3)_3 \cdot 26\text{H}_2\text{O}$ ) and 25 mL of a 0.2 M urea ( $\text{CO}(\text{NH}_2)_2$ ) water solution are combined in a beaker. This mixture was heated in a microwave system for less than 10 min.  $\text{Ga}_2\text{O}_3$  NCs are retrieved as a fine, black powder after this time inside the microwave. This powder is centrifuged several times while being rinsed with distilled water. The  $\text{CO}_2$  laser equipment was used to create the graphene nanopowder. A  $\text{CO}_2$  laser device with a 40 W maximum power and 400 mm/s maximum speed was employed. First, 170 m (5.0 mol) of DuPont Kapton Polyimide Film (TapeCase, USA) was thoroughly cleaned. The sheet was put on the laser cutter and subjected to 7.5 W of power traveling at 40 mm/s. A sizable amount (in mg) of graphene powder

was produced after the polyimide sheet was exposed to the laser beam over a sizable area Fig. 1 [14]. The oxide materials were next combined with graphene powder at various weight percentages, such as 5.0% and 10% of graphene. The combination was thoroughly ground for 5 min in the mortar, changing the color of the mixture to a light black hue. The product underwent an hour-long sintering procedure in an electric furnace set at  $400^\circ\text{C}$ .

### 2.2. Characterizations

A confocal Raman spectrometer (LAB RAM-HR800) coupled to a charge-coupled detector was also used to analyse the products (CCD). 20 mW of HeNe excitation light with a wavelength of 633 nm was employed. A backscattering setup with a spectral resolution of 0.8 cm was used for the Raman spectroscopy studies at room temperature. At varied irradiation times, the photocatalysis characteristics of MB were methodically examined. The absorbance spectra of the MB have two peaks at 490 and 970 nm. The calibration curve between the absorbance on the X-axis and dye concentration on the Y-axis was constructed using various dye concentrations of 5.0–10 mg/L of dye.

## 3. Results and discussions

### 3.1. Raman spectroscopy

Raman spectroscopy is sensitive to the lattice disorder of crystals as well as their degrees of crystallinity [15]. Three important vibrations appear that describe the surface defects of graphene as a carbonaceous material, identifying the impurities, and multilayers formation. The three vibrations appear in three bands: D, G, and 2D, respectively. The apparent D-band in graphene up to a certain level is due to the layered formation and further indicates crystalline defects. From Fig. 2, it is observed that the D band is higher compared to the G band. In the present graphene, the D/G intensity ratio expresses the induced high disordered layers [15]. The 2D to G intensity ratio indicates the multi-layered carbon in the as-prepared graphene [16,17]. The 2D- and G-bands are appearing strongly for  $\text{Ga}_2\text{O}_3/10\%\text{Gr}$ . For 30 min the combined samples were calcined at  $400^\circ\text{C}$ . This may reduce the disorder of the graphene that was surrounded by the oxide materials. It was observed that the redshift occurred for the 2D- and the D-band after the

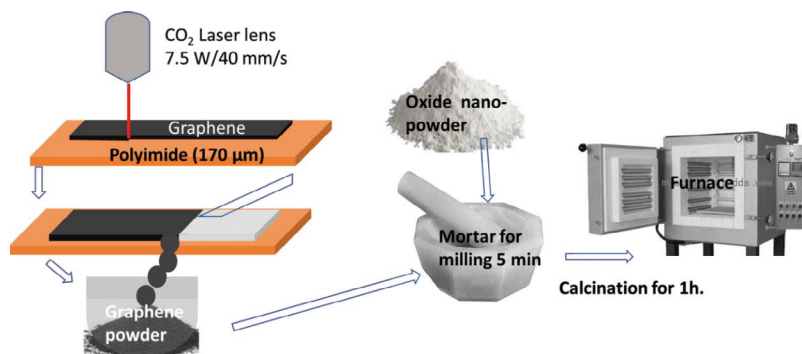


Fig. 1. Steps for preparing graphene powder by using a  $\text{CO}_2$  laser machine and preparing the  $\text{Ga}_2\text{O}_3$ -graphene composites.

addition of the oxide. Table 1 shows all Raman vibrations observed for the samples, and vibration modes reported in the literature [15,18,19]. However, the observed shift in the D-band and the 2D-band may be attributed to the interference between the oxide and the graphene at the interfaces, which may lead to the occurrence of new vibrations, as shown by the band observed at 1,050–1,094  $\text{cm}^{-1}$ .

3.2. Degradation studies

3.2.1. Dual adsorption and absorption studies

It is well knowledge that the amount of dye degradation is directly correlated with the optical absorbance values at a specific wavelength. A first experiment was conducted to determine the precise and direct correlation between this dye's concentration and absorption for this purpose. The association between the various MB concentrations and the absorbance calculated at that concentration for the primary peak of 664 nm is shown in Fig. 3. It was discovered that there is a linear, straight-line relationship between concentration and absorbance. The line is straight and goes through the origin; its slope is  $32 \pm 0.19 \text{ mg/L}$ , and its correlation coefficient  $R^2$  is 0.99.

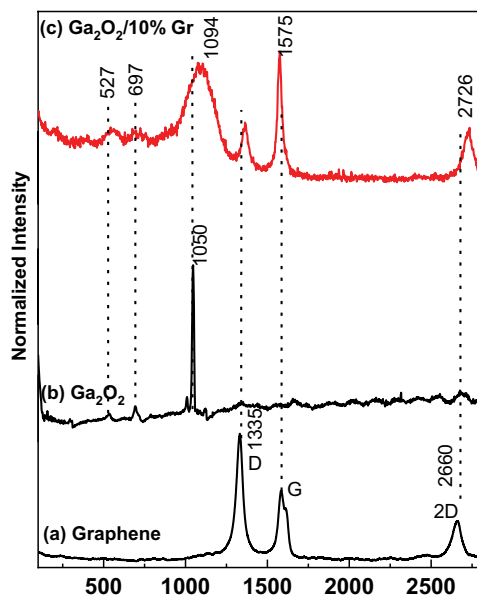


Fig. 2. Raman spectra for the prepared graphene, gallium oxide, and graphene-mixed gallium oxide.

The UV-vis spectrophotometer recorded this calibration curve. During the measurement of the UV-vis spectra, the dye concentration is directly given based on the calibration curve.

The efficiency ( $\eta$ ) of MB was calculated by the expression [20].

$$\eta\% = \frac{C_o - C_t}{C_o} \times 100 = \frac{A_o - A_t}{A_o} \times 100 \quad (1)$$

where  $C_o$ : initial MB concentration,  $C_t$ : residual MB concentration after time,  $A_o$ : initial MB absorbance,  $A_t$ : residual MB absorbance after time.

The adsorption studies have been done for 180 min, the efficiency ( $\eta$ ) was calculated using equation 1 for MB on the nanocomposites of  $\text{Ga}_2\text{O}_2/5\%\text{Gr}$ ,  $\text{Ga}_2\text{O}_2/10\%\text{Gr}$  with two different concentrations of methyl blue of 5 and 10 mg/L. This calculated efficiency is illustrated in Fig. 4. The figure shows that with increasing shaking time, the efficiency increases until reach to 26%, 25%, 32%, and 35% for  $\text{Ga}_2\text{O}_2/5\%\text{Gr}/5\text{MB}$ ,  $\text{Ga}_2\text{O}_2/5\%\text{Gr}/10\text{MB}$ ,  $\text{Ga}_2\text{O}_2/10\%\text{Gr}/5\text{MB}$  and  $\text{Ga}_2\text{O}_2/10\%\text{Gr}/10\text{MB}$ , respectively. For improving the degradation, a new step has been done which is photocatalytic study. The photocatalytic action of  $\text{Ga}_2\text{O}_2/5\%\text{Gr}$  and  $\text{Ga}_2\text{O}_2/10\%\text{Gr}$  nanoparticles (NPs) was examined by

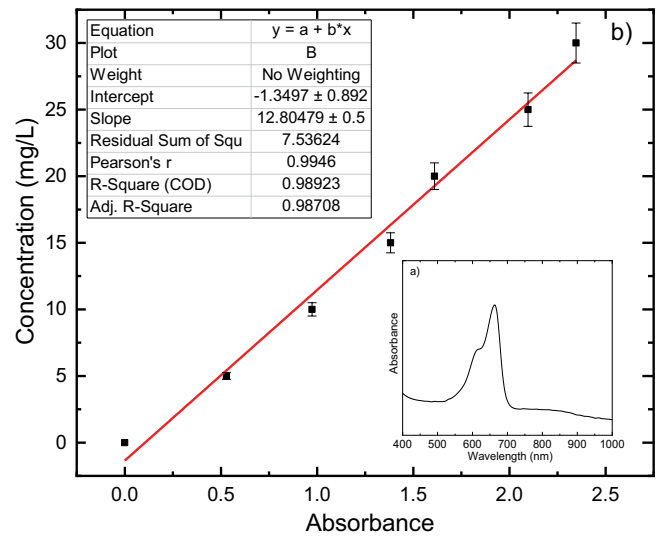


Fig. 3. Concentration vs. absorbance calibration curve for methylene blue dye in water solution our previous work [29].

Table 1

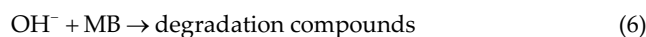
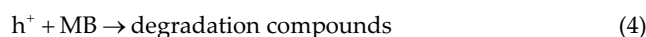
Raman vibration modes observed for graphene,  $\text{Ga}_2\text{O}_2/5\%\text{Gr}$ ,  $\text{Ga}_2\text{O}_2/10\%\text{Gr}$  nanocomposites

Vib. mode ( $\text{cm}^{-1}$ )	527	697	1,050	1,094	1,335	1,365	1,575	2,660	2,727
Sample									
Graphene	–	–	–	–	O	–	O	O	–
$\text{Ga}_2\text{O}_2$	O	O	O	–	–	–	–	–	–
$\text{Ga}_2\text{O}_2/10\%\text{Gr}$	O	O	–	O	O	–	O	–	O
Graphene [15,16]	–	–	–	–	O	–	O	O	–
$\beta\text{-Ga}_2\text{O}_2$ [17,18]	–	O	O	–	–	–	–	–	–

following the debasement of MB as an essential contamination display. It was discovered that the concentration of MB decreased as the illumination time increased, demonstrating the potential of Ga<sub>2</sub>O<sub>3</sub>/5%Gr and Ga<sub>2</sub>O<sub>3</sub>/10%Gr NPs to degrade MB under UV light. Additionally, the debasement process does not modify the position of MB's peak absorption wavelength (664 nm), which exposes the full debasement of the color without moving into additional toxic compounds [1]. This calculated efficiency is illustrated in Fig. 4. The figure shows that with increasing UV irradiation time, the efficiency increases until reach to 45%, 57%, 27% and 50% for Ga<sub>2</sub>O<sub>3</sub>/5%Gr/5 MB, Ga<sub>2</sub>O<sub>3</sub>/5%Gr/10 MB, Ga<sub>2</sub>O<sub>3</sub>/10%Gr/5 MB and Ga<sub>2</sub>O<sub>3</sub>/10%Gr/10 MB, respectively.

Typically, in a photocatalytic process, photo-induced molecular transformation or response happens at the surface of the NPs. When a photocatalyst is exposed to energy over its band gap, electrons move to the conduction band, and holes form in the valence band, which is the hypothesized mechanism of photocatalytic response on the production of an electron-hole pair and its aim. Hydroxyl radicals, which are highly oxidizing in nature, can be produced by the holes. Where the debasement process takes place, the

holes may react with dye and dynamic electrons [20]. As a result, the present sample instantly starts to deteriorate when exposed to light. Due to the formation of holes (h<sup>+</sup>) in the conduction band and electrons (e<sup>-</sup>) in the valence band, this will occur. Strong oxidizing and reducing agents are regarded as h<sup>+</sup> and e<sup>-</sup>, respectively. While the electrons work to diminish the oxygen adsorbed on the catalyst, the hole will either directly react with MB or it will react with water that has been added to our samples to form OH<sup>-</sup> radicals [1,21]. The reaction is represented by the following equations:



Methyl blue mass degraded per unit of NPs ( $q_t$ , mg/g) at a fixed time and at equilibrium state were calculated [22]:

$$q_t = (C_i - C_t) \frac{V}{W} \quad (7)$$

$$q_e = (C_i - C_e) \frac{V}{W} \quad (8)$$

where  $q_t$ : quantity of degraded MB capacity at time (t), mg/g,  $q_e$ : quantity of degraded MB at equilibrium state, mg/g,  $C_i$ : initial concentration of MB solution, mg/L,  $C_t$ : concentration of degraded at time (t), mg/L,  $C_e$ : equilibrium concentration of degraded MB, mg/L,  $V$ : solution volume, L and  $W$ : mass, g. Fig. 5 shows the effect of the contact time on the

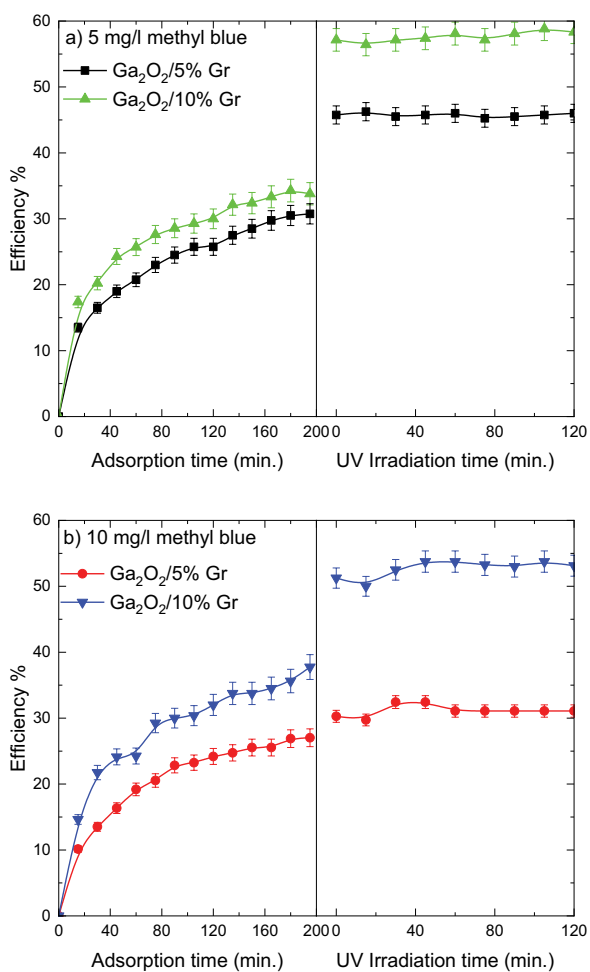


Fig. 4. Adsorption followed by photocatalytic efficiency of methylene blue on the nanocomposites of Ga<sub>2</sub>O<sub>3</sub>/5%Gr, Ga<sub>2</sub>O<sub>3</sub>/10%Gr with two different concentrations of methyl blue of (a) 5 and (b) 10 mg/L.

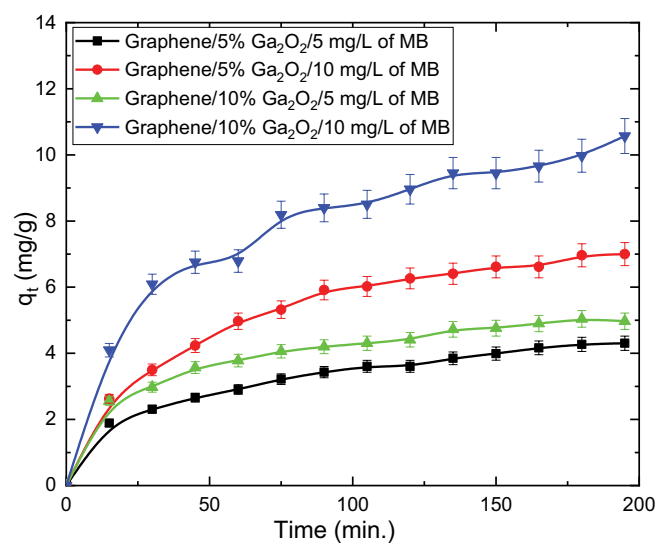


Fig. 5. Effect of the contact time on the adsorption capacity of methylene blue in the presence of Ga<sub>2</sub>O<sub>3</sub>/5%Gr, Ga<sub>2</sub>O<sub>3</sub>/10%Gr with two different concentrations of methyl blue of 5 and 10 mg/L.

adsorption capacity of MB in the presence of Ga<sub>2</sub>O<sub>3</sub>/5%Gr, Ga<sub>2</sub>O<sub>3</sub>/10%Gr with two different concentrations of methyl blue of 5 and 10 mg/L. It shows that, with increasing shaking time the adsorption capacity of MB increasing, moreover, the Ga<sub>2</sub>O<sub>3</sub>/10%Gr shows the highest adsorption capacity of MB.

3.2.2. Adsorption studies

For analyzing the results in the first 180 min, there are three models; pseudo-first-order, and (ii) second-order as well the intraparticle diffusion models were used [23].

$$\log(q_e - q_t) = \log q_e - K_1 \frac{t}{2.303} \text{ Pseudo-first-order model} \quad (9)$$

$$\frac{t}{q_t} = \frac{1}{(K_2 q_e^2)} + \frac{t}{q_e} \text{ Pseudo-second-order model} \quad (10)$$

$$q_t = K_{diff} \sqrt{t} + C \text{ Intraparticle diffusion} \quad (11)$$

Fig. 6 shows the pseudo-first-order kinetics model for the adsorption of MB in the presence of Ga<sub>2</sub>O<sub>3</sub>/5%Gr, Ga<sub>2</sub>O<sub>3</sub>/10%Gr with two different concentrations of methyl blue of 5 and 10 mg/L. On the other hand, the pseudo-second-order kinetics model for the adsorption of MB in the presence of Ga<sub>2</sub>O<sub>3</sub>/5%Gr, Ga<sub>2</sub>O<sub>3</sub>/10%Gr with two different concentrations of methyl blue of 5 and 10 mg/L as shown in Fig. 7. Moreover, Fig. 8 illustrates the intraparticle diffusion model for the adsorption of MB in the presence of Ga<sub>2</sub>O<sub>3</sub>/5%Gr, Ga<sub>2</sub>O<sub>3</sub>/10%Gr with two different concentrations of methyl blue of 5 and 10 mg/L. As a comparison of the R<sup>2</sup> values, it is concluded that the value of R<sup>2</sup> of pseudo-first-order kinetic model is higher than that values of pseudo-second-order kinetic model. Moreover, the difference between the determined and experimental for the pseudo-first-order is less than of the pseudo-second-order kinetic model as listed Table 2.

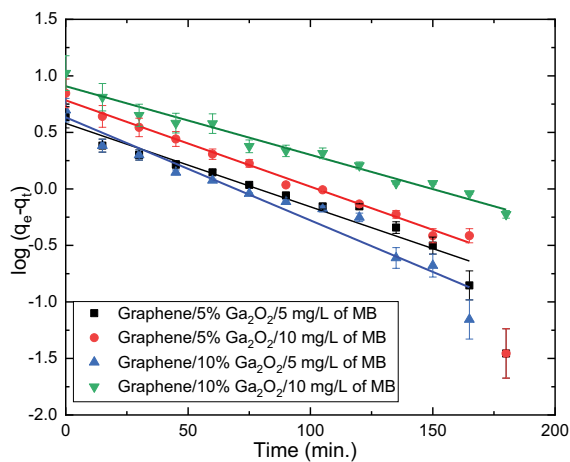


Fig. 6. Pseudo-first-order kinetics model for the adsorption of methylene blue in the presence of Ga<sub>2</sub>O<sub>3</sub>/5%Gr, Ga<sub>2</sub>O<sub>3</sub>/10%Gr with two different concentrations of methyl blue of 5 and 10 mg/L.

The Elovich equation is a different suggested equation for analyzing the adsorption of the researched substance. The afore-mentioned equation, Eq. (7), is frequently used in studies of the chemisorption of gases onto solids. Additionally, it can be used to research the solutes that are adsorbing from a liquid solution. The following expression represents the Elovich equation [24]:

$$q_t = \frac{\ln(\alpha\beta) + \ln(t)}{\beta} \quad (12)$$

where  $\alpha$ : initial sorption rate (mg/g-min),  $\beta$ : parameter of surface coverage and activation energy for chemisorption (g/mg). Fig. 9 shows plots of  $q_t$  vs.  $\ln(t)$  vs. time ( $t$ ) of MB in the presence of Ga<sub>2</sub>O<sub>3</sub>/5%Gr, Ga<sub>2</sub>O<sub>3</sub>/10%Gr with two different concentrations of methyl blue of 5 and 10 mg/L. The MB adsorption parameters in the presence of graphene/5%Ga<sub>2</sub>O<sub>3</sub> and graphene/10%Ga<sub>2</sub>O<sub>3</sub> illustrates in

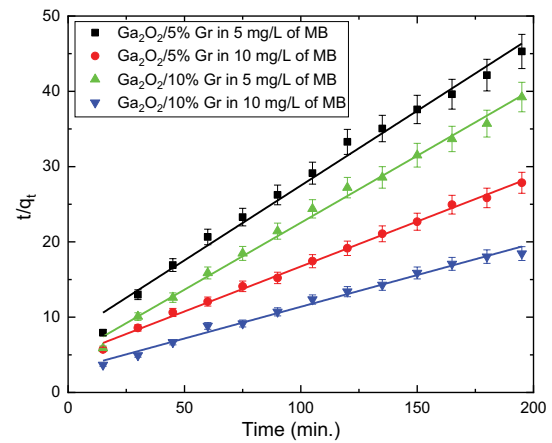


Fig. 7. Pseudo-second-order kinetics model for the adsorption of methylene blue in the presence of Ga<sub>2</sub>O<sub>3</sub>/5%Gr, Ga<sub>2</sub>O<sub>3</sub>/10%Gr with two different concentrations of methyl blue of 5 and 10 mg/L.

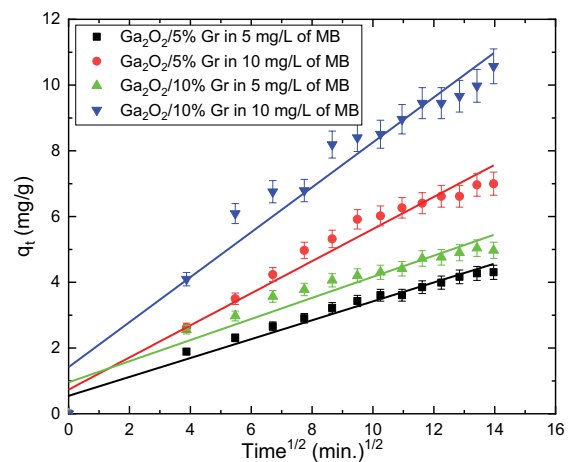


Fig. 8. Intraparticle diffusion model for the adsorption of methylene blue in the presence of Ga<sub>2</sub>O<sub>3</sub>/5%Gr, Ga<sub>2</sub>O<sub>3</sub>/10%Gr with two different concentrations of methyl blue of 5 and 10 mg/L.

Table 2  
Two different concentrations of methylene blue adsorption parameters in the presence of Ga<sub>2</sub>O<sub>3</sub>/5%Gr and Ga<sub>2</sub>O<sub>3</sub>/10%Gr

Adsorbent	MB (mg/L)	Pseudo-first-order kinetic model				Pseudo-second-order kinetic model				Intraparticle diffusion kinetic model			Elovich kinetic model			
		$q_{t,exp}$	$q_{t,cal}$	$q_{t,exp} - q_{t,cal}$	$k_1$	$R^2$	$q_{t,cal}$	$q_{t,exp} - q_{t,cal}$	$k_2 \times 10^{-3}$	$R^2$	$C$	$k_{diff}$	$R^2$	$\alpha$	$\beta$	$R^2$
Ga <sub>2</sub> O <sub>3</sub> /5%Gr	5	4.30	3.80	0.5	0.017	0.95	5.04	0.74	5.18	0.99	0.29	0.546	0.97	0.35	1.01	0.98
Ga <sub>2</sub> O <sub>3</sub> /5%Gr	10	7.00	6.08	0.92	0.018	0.99	8.40	1.40	2.96	0.99	0.49	0.734	0.96	0.47	0.56	0.99
Ga <sub>2</sub> O <sub>3</sub> /10%Gr	5	4.97	4.30	0.67	0.021	0.94	5.62	0.65	6.64	0.99	0.32	0.957	0.92	0.75	0.99	0.98
Ga <sub>2</sub> O <sub>3</sub> /10%Gr	10	10.57	8.10	2.47	0.014	0.97	11.90	1.33	2.39	0.99	0.68	1.418	0.95	0.90	0.42	0.98

Table 2. The adsorption process may be broken down into a number of processes, including (i) solution bulk transport, (ii) film diffusion, (iii) particle diffusion, and (iv) particle and solid's surface sorption and desorption [25]. While occurring quickly, the processes (ii) and (iii) are referred to as rate-limiting processes. Boyd recommended using the following mathematically written model to study the diffusion mechanism during the adsorption process [26]:

$$B_t = -0.4977 - \ln\left(1 - \frac{q_t}{q_e}\right) \tag{13}$$

Eq. (8) is a mathematical function of  $(q_t/q_e)$ , this ratio provides the adsorbate adsorbed fraction at different shaker times. Plots of  $B_t$  vs. the time ( $t$ ) of MB in the presence of Ga<sub>2</sub>O<sub>3</sub>/5%Gr, Ga<sub>2</sub>O<sub>3</sub>/10%Gr with two different concentrations of methyl blue of 5 and 10 mg/L is shown in Fig. 10. In the event that a linear plot of  $B_t$  vs.  $t$  passes through the

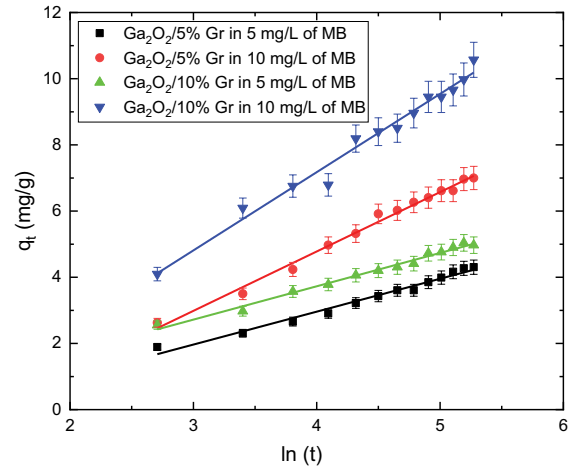


Fig. 9. Plots of  $q_t$  vs.  $\ln(t)$  vs. time ( $t$ ) of methylene blue in the presence of Ga<sub>2</sub>O<sub>3</sub>/5%Gr, Ga<sub>2</sub>O<sub>3</sub>/10%Gr with two different concentrations of methyl blue of 5 and 10 mg/L.

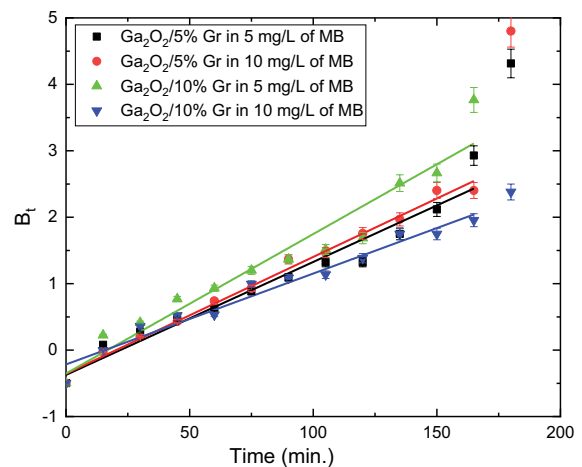


Fig. 10. Plots of  $B_t$  vs. the time ( $t$ ) of methylene blue in the presence of Ga<sub>2</sub>O<sub>3</sub>/5%Gr, Ga<sub>2</sub>O<sub>3</sub>/10%Gr with two different concentrations of methyl blue of 5 and 10 mg/L.

Table 3

Degradation efficiency of methylene blue using Ga<sub>2</sub>O<sub>2</sub>/5%Gr, Ga<sub>2</sub>O<sub>2</sub>/10%Gr in this study was compared to previously published work

Samples	Methylene blue	Degradation (%)	Irradiation	Time (min)	References
Ga <sub>2</sub> O <sub>2</sub> /5%Gr	5 mg/L	29	Adsorption	200	Current work
		45	UV irradiation	120	
	10 mg/L	25	Adsorption	200	
		22	UV irradiation	120	
Ga <sub>2</sub> O <sub>2</sub> /10%Gr	5 mg/L	32	Adsorption	200	
		57	UV irradiation	120	
	10 mg/L	35	Adsorption	200	
		50	UV irradiation	120	
WO <sub>3</sub> NPs	10 mg/L	55	NIR light	50	[30]
		43	UV		
ZnO at 0.15 Torr	1 × 10 <sup>-6</sup> M	81	Sun simulator	90	[31]
ZnO at 0.30 Torr		80			
ZnO at 0.70 Torr		65			
ZnO at 1.00 Torr		56			
ZrO <sub>2</sub> NPs	5 mg/L	30	UV light	240	[29]
ZrO <sub>2</sub> /G5 NPs		30			
ZrO <sub>2</sub> /G10 NPs		80			
ZrO <sub>2</sub> NPs		20			
ZrO <sub>2</sub> /G5 NPs	10 mg/L	60			
ZrO <sub>2</sub> /G10 NPs		60			

origin, the Boyd model states that. This indicates that the particle diffusion process is under process control. On the other hand, the diffusion might be thought of as the process's rate-limiting step. The two different concentrations of MB adsorption parameters in the presence of graphene/5%Ga<sub>2</sub>O<sub>2</sub> and graphene/10%Ga<sub>2</sub>O<sub>2</sub> illustrates in Table 2.

### 3.2.3. Comparison of performance with reported metallic oxides NPs

This section illustrates a comparison between the current work and the photocatalytic degradation of MB in the presence of several nanomaterials. Since graphene is thought to be robust, thin, and chemically resistant, previous research have referred to it as the "ultimate" RO membrane [27]. The production and application of graphene oxide nanocomposites for heavy metal, toxic organic pollutant, and antibacterial applications has attracted a lot of attention. After 90 min of exposure to direct sunlight at 2 × 10<sup>-5</sup> M MB concentrations and Ti-S-500 nanoparticle samples, 44% of the degradation is reached [28]. In contrast, 80% of the G10 for MB concentrations of 5 mg/L would degrade in the current samples if the time limit was 240 min [29]. Table 3 compares how MB dye degrades catalytically for various materials. In comparison to other published materials, the outcome provided here exhibits a superior behavior.

## 4. Conclusions

In conclusion, the phase of the Ga<sub>2</sub>O<sub>2</sub>-graphene heterostructure nanocomposite was fabricated to examine the interaction between the oxide and graphene heterojunction

on the degradation of the methyl blue dye. A CO<sub>2</sub> laser was used to create the flawed graphene, which was then embedded with Ga<sub>2</sub>O<sub>2</sub>. With a heterojunction of Ga<sub>2</sub>O<sub>2</sub>, the impact of graphene content was examined at 5% and 10% weight. The findings of catalysis tests showed that the heterojunction of Ga<sub>2</sub>O<sub>2</sub> with an appropriate concentration of graphene resulted in an improvement. The findings indicated that the photocatalytic application of the binary phase of Ga<sub>2</sub>O<sub>2</sub>/graphene toward the decomposition of methyl blue is promising.

## Acknowledgment

The authors extend their appreciation to the Deanship of Scientific Research at the University of Tabuk for funding this work through Research Group RGP-S-1443-0046.

## References

- [1] M. Rashad, T.A. Hamdalla, A.A.A. Darwish, S.M. Seleim, High performance efficiency of water purification using Cr<sub>2</sub>O<sub>3</sub> nanoparticles synthesized by thermal combustion technique, *Mater. Res. Express*, 6 (2019) 065048, doi: 10.1088/2053-1591/ab076c.
- [2] M. Rashad, H.A. Al-Aoh, Promising adsorption studies of bromophenol blue using copper oxide nanoparticles, *Desal. Water Treat.*, 139 (2019) 360–368.
- [3] N.M. Shaalan, M. Rashad, A.H. Moharram, M.A. Abdel-Rahim, Promising methane gas sensor synthesized by microwave-assisted Co<sub>3</sub>O<sub>4</sub> nanoparticles, *Mater. Sci. Semicond. Process.*, 46 (2016) 1–5.
- [4] F. Ye, A. Ohmori, C. Li, New approach to enhance the photocatalytic activity of plasma sprayed TiO<sub>2</sub> coatings using pn junctions, *Surf. Coat. Technol.*, 184 (2004) 233–238.

- [5] M.N. Chong, B. Jin, C.W.K. Chow, C. Saint, Recent developments in photocatalytic water treatment technology: a review, *Water Res.*, 44 (2010) 2997–3027.
- [6] M. Rashad, N.M. Shaalan, A.M. Abd-Elnaiem, Degradation enhancement of methylene blue on ZnO nanocombs synthesized by thermal evaporation technique, *Desal. Water Treat.*, 57 (2016) 26267–26273.
- [7] G. Kotan, F. Kardaş, Ö.A. Yokuş, O. Akyıldırım, H. Saral, T. Eren, M.L. Yola, N. Atar, A novel determination of curcumin via Ru@Au nanoparticle decorated nitrogen and sulfur-functionalized reduced graphene oxide nanomaterials, *Anal. Methods*, 8 (2016) 401–408.
- [8] M.L. Yola, N. Atar, T. Eren, H. Karimi-Maleh, S. Wang, Correction: sensitive and selective determination of aqueous triclosan based on gold nanoparticles on polyoxometalate/reduced graphene oxide nanohybrid, *RSC Adv.*, 5 (2015) 72590–72591.
- [9] N. Atar, T. Eren, M.L. Yola, H. Gerengi, S. Wang, Fe@Ag nanoparticles decorated reduced graphene oxide as ultrahigh capacity anode material for lithium-ion battery, *Ionics (Kiel)*, 21 (2015) 3185–3192.
- [10] N. Atar, T. Eren, M.L. Yola, Ultrahigh capacity anode material for lithium ion battery based on rod gold nanoparticles decorated reduced graphene oxide, *Thin Solid Films*, 590 (2015) 156–162.
- [11] L. Shao, X. Duan, Y. Li, F. Zeng, H. Ye, P. Ding, Two-dimensional Ga<sub>2</sub>O<sub>3</sub> monolayer with tunable band gap and high hole mobility, *Phys. Chem. Chem. Phys.*, 23 (2021) 666–673.
- [12] L. Zhao, S. Lam, Y. Thai, J. Sin, Fe<sub>2</sub>WO<sub>6</sub> coupling on cube-like SrTiO<sub>3</sub> as a highly active S-scheme heterojunction composite for visible light photocatalysis and antibacterial applications, *Environ. Technol. Innovation*, 28 (2022) 102941, doi: 10.1016/j.eti.2022.102941.
- [13] Y.-H. Chin, J.-C. Sin, S.-M. Lam, H. Zeng, H. Lin, H. Li, L. Huang, A.R. Mohamed, 3-D/3-D Z-Scheme heterojunction composite formed by Marimo-like Bi<sub>2</sub>WO<sub>6</sub> and Mammillaria-like ZnO for expeditious sunlight photodegradation of dimethyl phthalate, *Catalysts*, 12 (2022) 1427, doi: 10.3390/catal12111427.
- [14] N.M. Shaalan, M. Rashad, C. Awada, Synergistic effect of NiO-Ga<sub>2</sub>O<sub>3</sub>-graphene heterostructures on Congo red photodegradation in water, *Separations*, 9 (2022) 201, doi: 10.3390/separations9080201.
- [15] M.M. Lucchese, F. Stavale, E.H.M. Ferreira, C. Vilani, M.V.O. Moutinho, R.B. Capaz, C.A. Achete, A. Jorio, Quantifying ion-induced defects and Raman relaxation length in graphene, *Carbon N.Y.*, 48 (2010) 1592–1597.
- [16] A.C. Ferrari, Raman spectroscopy of graphene and graphite: disorder, electron-phonon coupling, doping and non-adiabatic effects, *Solid State Commun.*, 143 (2007) 47–57.
- [17] N.M. Shaalan, F. Ahmed, S. Kumar, A. Melaibari, P.M.Z. Hasan, A. Aljaafari, Monitoring food spoilage based on a defect-induced multiwall carbon nanotube sensor at room temperature: preventing food waste, *ACS Omega*, 5 (2020) 30531–30537.
- [18] D. Dohy, G. Lucazeau, A. Revcolevschi, Raman spectra and valence force field of single-crystalline β Ga<sub>2</sub>O<sub>3</sub>, *J. Solid State Chem.*, 45 (1982) 180–192.
- [19] T. Onuma, S. Fujioka, T. Yamaguchi, Y. Itoh, M. Higashiwaki, K. Sasaki, T. Masui, T. Honda, Polarized Raman spectra in β-Ga<sub>2</sub>O<sub>3</sub> single crystals, *J. Cryst. Growth*, 401 (2014) 330–333.
- [20] H. Zhu, R. Jiang, Y. Fu, Y. Guan, J. Yao, L. Xiao, G. Zeng, Effective photocatalytic decolorization of methyl orange utilizing TiO<sub>2</sub>/ZnO/chitosan nanocomposite films under simulated solar irradiation, *Desalination*, 286 (2012) 41–48.
- [21] S. Farhadi, K. Pourzare, S. Sadeghinejad, Simple preparation of ferromagnetic Co<sub>3</sub>O<sub>4</sub> nanoparticles by thermal dissociation of the [CoII(NH<sub>3</sub>)<sub>6</sub>](NO<sub>3</sub>)<sub>3</sub> complex at low temperature, *J. Nanostruct. Chem.*, 3 (2013) 16, doi: 10.1186/2193-8865-3-16.
- [22] A. Faisal, W.M.A.W. Daud, M.A. Ahmad, R. Radzi, Using cocoa (*Theobroma cacao*) shell-based activated carbon to remove 4-nitrophenol from aqueous solution: kinetics and equilibrium studies, *Chem. Eng. J.*, 178 (2011) 461–467.
- [23] H.A. Al-Aoh, M.J. Maah, R. Yahya, M.R. Bin Abas, A comparative investigation on adsorption performances of activated carbon prepared from coconut husk fiber and commercial activated carbon for Acid red 27 dye, *Asian J. Chem.*, 25 (2013) 9582, doi: 10.14233/ajchem.2013.15082A.
- [24] Y. Bulut, Z. Tez, Adsorption studies on ground shells of hazelnut and almond, *J. Hazard. Mater.*, 149 (2007) 35–41.
- [25] G. Akkaya, A. Özer, Biosorption of Acid red 274 (AR 274) on *Dicranella varia*: determination of equilibrium and kinetic model parameters, *Process Biochem.*, 40 (2005) 3559–3568.
- [26] H. Yan, J. Hou, Z. Fu, B. Yang, P. Yang, K. Liu, M. Wen, Y. Chen, S. Fu, F. Li, Growth and photocatalytic properties of one-dimensional ZnO nanostructures prepared by thermal evaporation, *Mater. Res. Bull.*, 44 (2009) 1954–1958.
- [27] M. Khan, M.N. Tahir, S.F. Adil, H.U. Khan, M. Rafiq H. Siddiqui, A.A. Al-warthan, W. Tremel, Graphene based metal and metal oxide nanocomposites: synthesis, properties and their applications, *J. Mater. Chem. A*, 3 (2015) 18753–18808.
- [28] A. Kundu, A. Mondal, Photodegradation of methylene blue under direct sunbeams by synthesized anatase titania nanoparticles, *SN Appl. Sci.*, 1 (2019) 1–17.
- [29] N.M. Shaalan, M. Rashad, O. Saber, A. Alshoabi, C. Awada, A comprehensive photocatalysis study of promising zirconia/laser-induced graphene nanocomposite for wastewater treatment-based methylene blue pollution, *Separations*, 9 (2022) 185, doi: 10.3390/separations9080185.
- [30] X. Yin, L. Liu, F. Ai, Enhanced photocatalytic degradation of methylene blue by WO<sub>3</sub> nanoparticles under NIR light irradiation, *Front. Chem.*, 9 (2021) 1–9.
- [31] M. Rashad, N.M. Shaalan, A.M. Abd-Elnaiem, Degradation enhancement of methylene blue on ZnO nanocombs synthesized by thermal evaporation technique, *Desal. Water Treat.*, 57 (2016) 26267–26273.